Evolution of the bootstrap current profile during the type I ELM cycle of JET-ILW H-mode plasmas

L. Horvath[1,2], C.F. Maggi[2], F.J. Casson[2], L. Frassinetti[3],
M.G. Dunne[4], J. Hobirk[4], I. Lupelli[2], K.J. Gibson[1] and JET Contributors*

EUROfusion Consortium, JET, Culham Science Centre, Abingdon OX14 3DB, UK
[1] *York Plasma Institute, Department of Physics, University of York, York, YO10 5DD, UK*
[2] *CCFE, Culham Science Centre, Abingdon, OX14 3DB, UK*
[3] *Division of Fusion Plasma Physics, KTH Royal Institute of Technology, Stockholm SE*
[4] *Max-Planck-Institut für Plasmaphysik, D-85748 Garching, Germany*
**See the Appendix of F. Romanelli et al., Proceedings of the 25th IAEA Fusion Energy Conference 2014, Saint Petersburg, Russia*

1. Introduction The understanding of the physical processes governing the behaviour of the edge pedestal structure is crucial in order to predict the plasma performance in future devices such as ITER. A well-known theory which explains the stability conditions in the pedestal is the peeling-ballooning (P-B) model [1]. In this model the bootstrap current, which can be efficiently driven by the steep pressure gradient at the plasma edge, plays a crucial role: it can stabilise ballooning modes through reduced magnetic shear or drive peeling modes in the edge.

A recent study [2] has shown that the pedestal stability in JET with the new Be/W ITER-like wall (JET-ILW) is consistent with the P-B model in discharges with low D_2 gas rates. However, high D_2 gas rates are required in JET-ILW to increase the ELM frequency in order to achieve core W control over longer time scales [3]. At high gas rate and high beta, pre-ELM pedestals have been shown to be stable to P-B modes, but ELMs still occur experimentally [2].

In order to try to understand the origin of this discrepancy, in this contribution we study the evolution of the calculated edge bootstrap current profile (j_{BS}) during the type I ELM cycle. We consider the same dataset of [2], [4], namely power and gas scans, which allow decoupling of effects of β and D_2 gas injection on ∇p_e, thus on j_{BS}.

2. Bootstrap current calculation The j_{BS} is computed with the local neoclassical transport code NEO [5, 6], which solves the drift-kinetic equation with a full linearized Fokker-Planck collision operator including all inter-species collisions. This approach provides a more accurate estimation of j_{BS} than using the Sauter-formula [7], [8], especially at high collisionality ($\nu*$), where the Sauter-formula overestimates j_{BS} (by up to 100 %) compared to NEO [2].

The input for NEO are the plasma equilibrium (from EFIT), the electron (T_e) and ion (T_i) temperatures and the ion density, which are evaluated from fitted electron kinetic profiles from Thomson scattering (HRTS) measurements assuming equal electron and ion temperatures, constant line averaged Z_{eff} and Be as the intrinsic impurity. The HRTS profiles collected from a steady time window of the discharge are ELM-synchronised. The ELM cycle is divided into 20 % long intervals, as shown in figure 1. As 100 % corresponds to the ELM crash and 0 %

corresponds to the ELM crash of the preceding ELM cycle, the 0-20 % interval is excluded from the analysis as the profiles in this interval are dominated by the ELM crash. Composite profiles are taken from each 20 % bin and a modified tanh function [9] is fitted to both the electron temperature (T_e) and density (n_e) profiles. Examples of fitted n_e and T_e profiles are shown on figure 2c and 2d, respectively, for JET-ILW discharge #84797 (1.4 MA/1.7 T, $P_{\mathrm{IN}} \approx 4$ MW, low δ, $\Gamma_D = 2.8 \cdot 10^{21}$ e/s). The time evolution of the j_{BS} profile through the ELM cycle for this discharge is shown in figure 2a, showing a similar time evolution to ∇p_e, as expected.

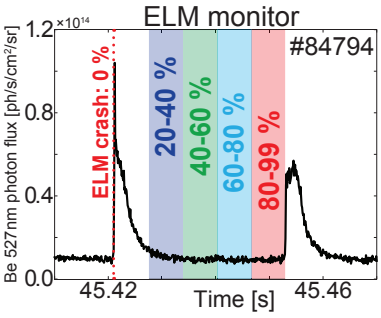

Figure 1: *ELM cycle is normalized to a relative time scale (from 0 % to 100 %) and divided into 20 % long intervals.*

3. Impact of n_e, T_e, Z_{eff} uncertainties on j_{BS} profile The uncertainty of the j_{BS} profiles on the input parameters n_e, T_e, Z_{eff} has been investigated with NEO. For this purpose, "modulated" n_e and T_e profiles are created where each parameter (width, height, position and slope) is substituted with a Gaussian random number. The mean and variance of the Gaussian random numbers are given by the mean and variance of the parameter estimates of the mtanh fit. The j_{BS} profile is then calculated several times (~ 50) using different "modulated" profiles. The line averaged Z_{eff} is varied between the experimental uncertainties of ± 10 %. The result of the sensitivity analysis is shown in figure 3, where all three parameters (n_e, T_e, Z_{eff}) are modulated within their uncertainties. The percentile of the resulting j_{BS} profiles gives the 1σ and 2σ error bars, which are visible in figure 3 in red and blue, respectively. Tests where only one input parameter was "modulated", have shown that the uncertainty in j_{BS} is dominated by the uncertainty of the T_e profiles. This is likely to be due to the higher uncertainty of the T_e profiles in this dataset. In the following figures the 1σ error bars will be used.

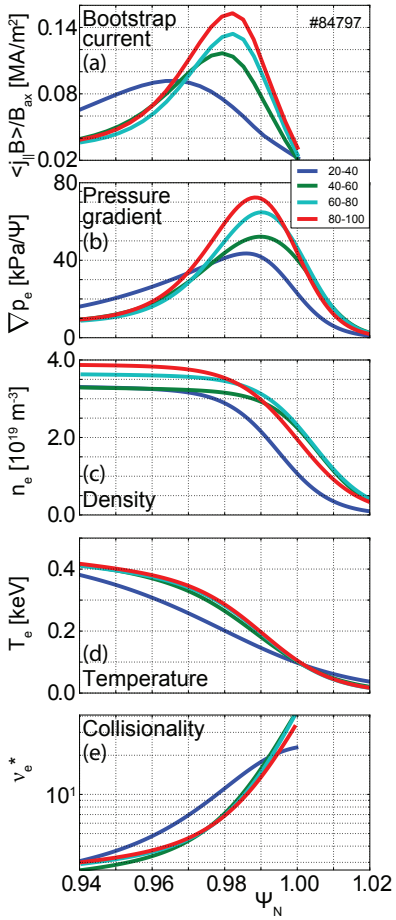

Figure 2: *Time evolution of (a) j_{BS}; (b) ∇p_e; (c) n_e; (d) T_e; (e) $\nu*$ profiles in #84797.*

4. Inter-ELM j_{BS} evolution The time evolution of the j_{BS} profiles (see figure 2a) is evaluated for the discharges in the dataset: 1.4 MA/1.7 T, low triangularity, $P_{sep} = 4 \rightarrow 14$ MW, gas injection rate: $2.8 \rightarrow 18 \cdot 10^{21}$ e/s, $\beta_N = 1.2 \rightarrow 2.8$, $f_{\mathrm{ELM}} = 12 \rightarrow 120$ Hz. The pedestal pressure varies between $p_{e,PED} = 1.3 \rightarrow 3$ kPa in the dataset. At a given P_{sep}, $p_{e,PED}$ is reduced with increasing gas rate. The pedestal collisionality ($\nu_{e,PED}$) is mainly driven by the variation in the pedestal top temperature [2] and varies between $\nu_{e,PED} = 0.3 \rightarrow 4.5$.

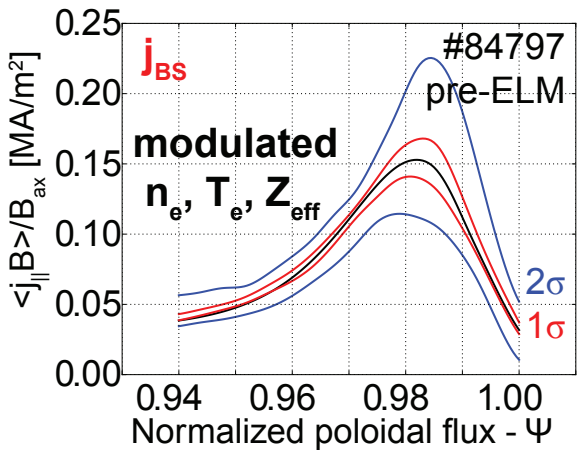

Figure 3: *1σ and 2σ error bars of the j_{BS} profile as a result of the sensitivity analysis to n_e, T_e and Z_{eff}.*

The evolution of the peak j_{BS} is shown in figure 4 at constant net power through the separatrix (P_{sep}) comparing low vs. high gas rate cases. At low gas injection (where the pre-ELM stability was consistent with the P-B model), the peak j_{BS} continuously increases during the ELM cycle. At medium and high gas rate (where the pedestals were stable against P-B modes just before the ELM crash) the peak j_{BS} is roughly constant throughout the ELM cycle. At low power ($P_{\text{sep}} \sim 4$ MW) in figure 4a, j_{BS} is reduced due to the lower T_e and thus higher $\nu*$, but the peak j_{BS} time evolution at low vs. high gas rate is similar to that at high P_{sep}

It is interesting to compare the inter-ELM j_{BS} evolution to that of the separate drives of ∇p_e, namely the temperature and density gradients, as shown in figure 5, where all values are normalized to the pre-ELM phase. For all shots of the dataset, experimentally we observe that peak j_{BS}, ∇p_e and ∇T_e have always the same time evolution, even if ∇n_e may differ in evolution. Figure 5a (low gas) shows a case where ∇n_e, ∇T_e and ∇p_e evolve similarly. In figure 5b (high gas), ∇n_e evolves differently to ∇p_e and ∇T_e. The latter behaviour is typical regarding the whole dataset, which is likely to be due to that the ∇T_e term in ∇p_e is higher than the ∇n_e term.

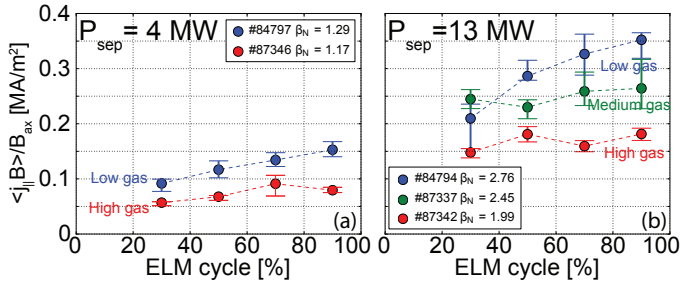

Figure 4: *j_{BS} evolution during the ELM cycle for discharges at low and high gas rates at constant P_{sep}: (a) lowest power and (b) highest power of the power and gas scans dataset.*

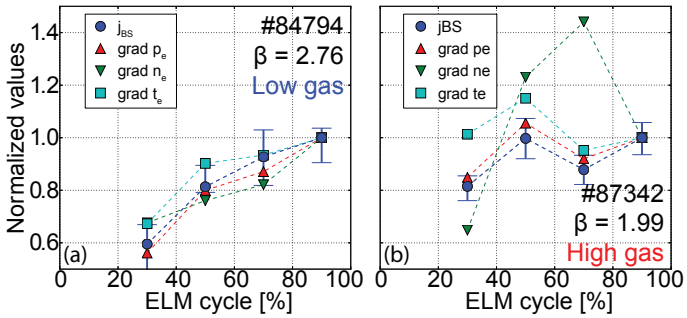

Figure 5: *The evolution of peak j_{BS} and the peak of p_e, n_e, T_e gradients at low and high gas at high input power. All values are normalized to the pre-ELM phase.*

In this study we have assumed j_{BS} to evolve in time following the pressure gradient without a delay, that is, ignoring current diffusion in the pedestal region. This assumption can be tested by estimating the resistive time scale for current diffusion in the edge transport barrier: $\tau_{res} \approx \mu_0 \Delta^2_{PED}/\eta_{Spitz}$, where μ_0 is the vacuum permeability, η_{Spitz} is the Spitzer resistivity and Δ_{PED} is the pedestal with which of the order of 2 cm. τ_{res} is estimated in two cases for low and high $\nu*$ pedestals of the power and gas scan (see table 1). As $\tau_{ELM} \gg \tau_{res}$, this simple estimate shows that a significant time delay of the edge current with respect to ∇p_e is unlikely. Therefore, it is unlikely that current diffusion in the pedestal could explain the discrepancy with the P-B model reported for high gas, high β discharges in [2].

	$T_{e,PED}$	η_{Spitz} @ max ∇T_e	ν_e* @ max ∇T_e	τ_{res}	τ_{ELM}
Low gas (#84794)	0.9 keV	$2.5{\cdot}10^{-7}\Omega$m	1	$\approx$ 2 ms	$\approx$ 28 ms
High gas (#87342)	0.6 keV	$3.5{\cdot}10^{-7}\Omega$m	4	$\approx$ 1.5 ms	$\approx$ 8 ms

Table 1: *Estimated resistive timescale of two discharges at the highest power in the power scan at low (low $\nu*$) and high gas (high $\nu*$).*

5. Conclusions and future work The present analysis has shown that in JET-ILW type I ELMy H-modes at low gas rate the peak j_{BS} continuously increases during the ELM cycle. In contrast, with increasing gas rate the peak j_{BS} tends to saturate during the ELM cycle, in agreement with previous analysis in JET-C [10]. The short resistive time scales for current diffusion in the pedestal indicate that the delay of edge current with respect to the pressure gradient is probably very small, thus it could not explain the ELM trigger. The time evolution of j_{BS} closely follows that of ∇p_e and ∇T_e, even if ∇n_e may differ in evolution. The uncertainty in the j_{BS} profiles with respect to to n_e, T_e and Z_{eff} is dominated by the uncertainty in T_e in this dataset. Future work will include, modelling of the Ohmic current contribution to the total edge current and its comparison with the edge current derived by EFIT reconstructions with kinetic constraints [11]. The impact of j_{BS} uncertainty on edge stability analysis will be also investigated.

This work was supported by the Engineering and Physical Sciences Research Council [EP/L01663X/1]. This work has been carried out within the framework of the EUROfusion Consortium and has received funding from the Euratom research and training programme 2014-2018 under grant agreement No 633053. The views and opinions expressed herein do not necessarily reflect those of the European Commission.

References

[1] P.B. Snyder et al., Physics of Plasmas **9**, 2037 (2002)
[2] C.F. Maggi et al., Nuclear Fusion **55**, 113031 (2015)
[3] M.N.A. Beurskens et al., Plasma Physics and Controlled Fusion **55**, 124043 (2013)
[4] C.D. Challis et al., Nuclear Fusion **55**, 053031 (2015)
[5] E. Belli et al., Plasma Physics and Controlled Fusion **50**, 095010 (2008)
[6] E. Belli et al., Plasma Physics and Controlled Fusion **54**, 015015 (2012)
[7] O. Sauter et al., Physics of Plasmas **6**, 2834 (1999)
[8] O. Sauter et al., Physics of Plasmas **9**, 5140 (2002)
[9] R. Scannell et al., Review of Scientific Instruments **82**, 053501 (2011)
[10] S. Saarelma et al., Nuclear Fusion **53**, 123012 (2013)
[11] L.C Appel et al., 33rd EPS Conference on Plasma Physics **30I**, P2.184 (2006)